

Topological states switching and group velocity control in two-dimensional non-reciprocal Hermitian photonic lattice

Yu Lin(林宇), Yuandan Wang(王元旦), Junhao Yang(杨俊豪), Yixuan Fu(符艺萱), and Xinyuan Qi(齐新元)
Citation: Chin. Phys. B, 2023, 32 (**11**): 114213. DOI: 10.1088/1674-1056/ad0621
Journal homepage: http://cpb.iphy.ac.cn; http://iopscience.iop.org/cpb

What follows is a list of articles you may be interested in

Generation of spectrally uncorrelated biphotons via fiber nonlinear quantum interference

Zhengtong Wei(卫正统), Chuan Qu(瞿川), Tian'an Wu(吴天安), Yuanyuan Li(李媛媛), Bo Li(李博), and Shenghai Zhang(张胜海)
Chin. Phys. B, 2023, 32 (**6**): 064202. DOI: 10.1088/1674-1056/acb767

Size effect on light propagation modulation near band edges in one-dimensional periodic structures

Yang Tang(唐洋), Jiajun Wang(王佳俊), Xingqi Zhao(赵星棋), Tongyu Li(李同宇), and Lei Shi(石磊)
Chin. Phys. B, 2023, 32 (**5**): 054201. DOI: 10.1088/1674-1056/acac0d

An improved method for the investigation of high-order harmonic generation from graphene

Zhong Guan(管仲), Lu Liu(刘璐), Guo-Li Wang(王国利)†, Song-Feng Zhao(赵松峰), Zhi-Hong Jiao(焦志宏), and Xiao-Xin Zhou(周效信)‡
Chin. Phys. B, 2020, 29 (**10**): 104206. DOI: 10.1088/1674-1056/abab76

Comment on “Band gaps structure and semi-Dirac point of two-dimensional function photonic crystals” by Si-Qi Zhang *et al.*

Hai-Feng Zhang(章海锋)
Chin. Phys. B, 2018, 27 (**1**): 014205. DOI: 10.1088/1674-1056/27/1/014205

Band gaps structure and semi-Dirac point of two-dimensional function photonic crystals

Si-Qi Zhang(张斯淇), Jing-Bin Lu(陆景彬), Yu Liang(梁禹), Ji Ma(马季), Hong Li(李宏), Xue Li(李雪), Xiao-Jing Liu(刘晓静), Xiang-Yao Wu(吴向尧), Xiang-Dong Meng(孟祥东)
Chin. Phys. B, 2017, 26 (**2**): 024208. DOI: 10.1088/1674-1056/26/2/024208

SPECIAL TOPIC — Celebrating the 100th Anniversary of Physics Discipline of Northwest University

Topological states switching and group velocity control in two-dimensional non-reciprocal Hermitian photonic lattice

Yu Lin(林宇), Yuandan Wang(王元旦), Junhao Yang(杨俊豪), Yixuan Fu(符艺萱), and Xinyuan Qi(齐新元)†

School of Physics, Northwest University, Xi'an 710127, *China*

(Received 30 June 2023; revised manuscript received 23 October 2023; accepted manuscript online 24 October 2023)

We proposed a model with non reciprocal coupling coefficients, in which the imaginary parts γ indicate the phase delay or exceed term. The distributions of band structure and the group velocity are both characterized as a function of the coupling. we studied the system's topological states and group velocity control. The results show that the movement and breaking of Dirac points exist in the energy band of the system. By changing the coupling coefficients, the conversion between any topological states corresponds to different Chern number. Topological edge states exist in topological non-trivial systems that correspond to the two different Chern numbers. Besides, it is also found that both the coupling coefficient and the wave vector can cause the oscillation of the pulse group velocity. At the same time, the topological state can suppress the amplitude of the group velocity profiles. Our findings enrich the theory of light wave manipulation in high-dimensional photonic lattices and provide a novel view for realizing linear localization and group velocity regulation of light waves, which has potential application in high-speed optical communication and quantum information fields.

Keywords: Dirac point, imaginary coupling, Chern number, group velocity

PACS: 42.70.Qs, 03.65.Vf, 42.79.Gn **DOI:** 10.1088/1674-1056/ad0621

1. Introduction

In recent years, topological photonic systems have attracted much attention from researchers, who have performed extensive studies on different topological photonic systems and achieved rich research results.[1] The study of topological photonic systems started in 1979, with the one-dimensional (1D) Su–Schrieffer–Heeger (SSH) model proposed by Su *et al.*[2] as a representative example, which realized topological phase transition through staggered coupling in the lattice.[3,4] Based on this, topological photonic devices have gradually attracted attention.[5–7] The SSH model has chiral and particle–hole symmetries,[8,9] and many novel phenomena have been discovered by studying the SSH model, such as topological invariants, topological phase transitions, edge states, etc.[10] With the progress of research, two-dimensional (2D) topological photonic systems have aroused great interest.[11] Quantum spin Hall effect (QSHE) and quantum valley Hall effect (QVHE) with time reversal symmetry can be realized in 2D photonic crystals.[12] QSHE can be realized in photonic crystals with strong spin–orbit coupling,[13] where spin-up and spin-down bands are inverted and separated by a band gap,[14] each spin sector having a nonzero Chern number with opposite signs. Therefore, there exist topologically protected edge states propagating along the system boundary, with opposite spins and directions. These edge states are immune to disorder-induced backscattering. QVHE can be realized in photonic crystals with honeycomb or hexagonal lattices,[15] where valleys correspond to two inequivalent Dirac cones at K and K' points. By introducing a staggered potential or breaking the sublattice symmetry,[16–18] a band gap can be opened at the Dirac points (DPs), and valleys acquire opposite Chern numbers.[19] Therefore, there exist topologically protected edge states propagating along the system boundary,[20,21] with opposite pseudospins and opposite group velocities. Both QVHE and QSHE based photonic topological insulators (PTIs) preserve time-reversal symmetry, and moreover, these PTIs can also host higher-order topological phases, such as second-order PTIs with corner states or third-order PTIs with hinge states.[22–26] In 2008, Haldane and Raghu proposed a method of breaking time reversal symmetry using magneto-optical materials,[27,28] which can realize one-way transmission of chiral edge states of light.[29,30] Wang *et al.*, successfully observed the robust one-way transmission of edge states in a 2D magnetic photonic crystal experiment.[31] However, most of the aforementioned 2D photonic systems require the time reversal symmetry breaking,[32] and are non Hermitian.[33–38] The studies in 2D non-reciprocal Hermitian photonic systems are still rarely reported.

In this paper, we constructed a 2D non-reciprocal Hermitian photonic lattice and studied theoretically and numerically the system's topological states and group velocity control. By changing the coupling coefficients, we analyzed the movement of DPs in the energy band structure, and the transformation between any topological states corresponding to different Chern numbers. Finally, we studied the impact of the topology on the group velocity.

†Corresponding author. E-mail: qixycn@nwu.edu.cn

© 2023 Chinese Physical Society and IOP Publishing Ltd

2. Topological state and dispersion curve

This section presents a 2D non-reciprocal coupled Hermitian photonic lattice and its unique properties. Figure 1 illustrates the structure of this lattice, which consists of two straight waveguides, A_n (blue) and B_n (red), forming a unit cell (red dashed box). Each unit cell has an imaginary coupling coefficient $\pm i\gamma$ between the two sublattices. The system can be modeled by coupled mode equations for the amplitudes a_n and b_n of the sublattices A and B, respectively:

$$-i\frac{da_n}{dz} = (t+i\gamma)b_n + \Delta(a_{n+1}+a_{n-1}) + \delta(b_{n+1} + b_{n-1}) - \sigma(b_{n+1}+b_{n-1})e^{-ik_y} + tb_{n-1}, \quad (1)$$

$$-i\frac{db_n}{dz} = (t-i\gamma)a_n + \Delta(b_{n+1}+b_{n-1}) + \delta(a_{n+1} + a_{n-1}) - \sigma(a_{n+1}+a_{n-1})e^{ik_y} + ta_{n+1}, \quad (2)$$

where n is the number of cells; Δ is the intralayer coupling coefficient; the interlayer coupling within a cell is non-reciprocal coupling with different imaginary coupling coefficients $t \pm i\gamma$; the interlayer coupling between cells is δ and σ. z represents the propagation distance of the wave packet, a_n, b_n are the field amplitudes of waveguides A_n, B_n.

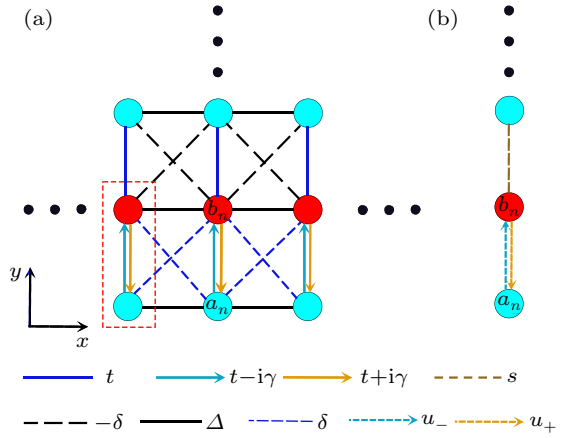


Fig. 1. (a) Schematic diagram of a 2D non-reciprocal Hermitian photonic lattice with two sites per cell. (b) The effective 1D chain structure of the model in (a).

For reduction of calculation, we simplify the Bloch Hamiltonian of the system to a 1D narrow-band chain model that is periodic along x and confined along y. Applying Bloch's theorem: $a_{n+1} = a_n e^{ik}$, $b_{n+1} = b_n e^{ik}$. In the momentum space, the equation can be written as

$$-i\frac{d}{dz}\begin{pmatrix} a_n \\ b_n \end{pmatrix} = H\begin{pmatrix} a_n \\ b_n \end{pmatrix}. \quad (3)$$

So the Hamiltonian $H(k)$ is written as

$$H(k) = \begin{pmatrix} m & u_+ + se^{-ik_y} \\ u_- + se^{ik_y} & m \end{pmatrix}, \quad (4)$$

where $m = 2\Delta\cos k_x$; $s = t - 2\sigma\cos k_x$; $u_\pm = u \pm i\gamma$ and $u = t + 2\delta\cos k_x$. For a given k_x, when $g \neq 0$ and $u_- \neq u_+$, equation (4) describes a 1D narrow-band chain model with non-reciprocal intra-cell coupling, as shown in Fig. 2(b). Analyzing the Bloch Hamiltonian reveals that it satisfies $H^\dagger = H$, indicating that the system is a Hermitian system with real energy spectra.

The dispersion relation can characterize and predict light transmission behavior in periodic photonic crystals. The Bloch Hamiltonian is given by Eq. (4), and a solution of the equation gave the dispersion relation, which was the expression of the system's energy band structure

$$E_\pm(k) = m \pm \sqrt{s^2 + e^{ik_y}su_+ + e^{-ik_y}su_- + u_+u_-}. \quad (5)$$

The dispersion relation can characterize and predict a 2D Brillouin zone (BZ). We divide it into several small squares and calculate each square's Berry curvature. We use the Chern number efficient method to simplify the calculation to solve whether the system has topological properties and transform the Berry curvature integral into a linear algebra problem.[49] This method is based on the Haldane model,[39–41] which assumes that the Hamiltonian can be expressed as

$$H(\boldsymbol{k}) = \sum_{i=1}^{4} d_i(\boldsymbol{k})\sigma_i, \quad (6)$$

where σ_i is the Pauli matrix and $d_i(\boldsymbol{k})$ is the real function. For such Hamiltonian quantities, the Berry curvature can be expressed as

$$F(\boldsymbol{k}) = 2\sum_{i<j}\varepsilon_{ijk}d_i(\boldsymbol{k})d_j(\boldsymbol{k}), \quad (7)$$

where ε_{ijk} is the Levi–Civita notation. The Berry curvature can be transformed into a linear problem by fitting $d_i(\boldsymbol{k})$ with a cubic function

$$F(\boldsymbol{k}) = [d(\boldsymbol{k}) \times \nabla_k d(\boldsymbol{k})] \cdot C, \quad (8)$$

where $d(\boldsymbol{k}) = [d_1(\boldsymbol{k}), d_2(\boldsymbol{k}), d_3(\boldsymbol{k})]$ and C is a constant. This linear problem can be solved by computing the dot product of $[d(\boldsymbol{k}) \times \nabla_k d(\boldsymbol{k})] \cdot C$ and C, and then integrating the result to obtain the Berry curvature. Finally, the Chern number can be calculated by substituting the Berry curvature into the integral formula for the Chern number.

The 2D non-reciprocal Hermitian system can be solved for whether it has topological properties by the above stale efficient method. We solve the topological states of the system separately when $\delta = \sigma$ and $\delta \neq \sigma$. When $\delta = \sigma$, the coupling coefficient $\Delta = 0$, $t = 0.5$ are fixed, and the Chern number of the system is calculated. The state is determined numerically, and the calculation results show that when the coupling coefficient $\delta = 0.5$ and $\gamma = 0$, $C = -2$, corresponding to a topological non-trivial state; when the coupling coefficient $\delta < 0.5$ and $\gamma > 0.3$, $C = -1$, corresponding to another topological

non-trivial state; when the coupling coefficient $\delta > 0.5$ and $\gamma > 0.3$, $C = 0$, corresponding to a trivial topological state. The robustness of the topological state is further calculated, and it is found that the topological state remains unchanged when $\Delta \in [0, 0.1]$.

When $\delta \neq \sigma$, the coupling coefficient $\Delta = 0.5$, $\delta = -1$, $t = 2$, $\sigma = 1$ is fixed, and the Chern number of the system is calculated. It is found that $C = 0$, regardless of the value of the imaginary coupling coefficient γ, implies that the system is in a topologically trivial state. For a fixed coupling constant $\Delta = 0$, $\delta = -1$, $t = 2$, $\sigma = 1$, the band structure of the Bloch Hamiltonian $H(k)$ is shown in Figs. 2(a)–2(c), where we plot the dispersion relation as a function of the wave vectors k_x and k_y.

When the intralayer coupling constant $\Delta = 0$, the system is chiral symmetric and preserves $CH(k)C^{-1} = -H(k)$. The band structure of the Bloch Hamiltonian $\gamma = 0$ is shown in Fig. 2(a); due to the chiral symmetry of the system, the upper and lower bands are symmetric, and there are two band inversion points at $(k_x, k_y) = (\pi/2, \pi/2)$, $(k_x, k_y) = (-\pi/2, -\pi/2)$. Because of the imaginary coupling constant $\gamma = 0$, the bands are also symmetric about the origin, and there are three DPs located at the edge (A_2, A_3) and center (A_1) of the BZ, with the edge DPs being symmetric about the origin $(k_x, k_y) = (0, 0)$. The 2D Dirac states reported to date are distributed only at high symmetry points in the BZ, and the low-energy dispersion of these Dirac states is isotropic due to symmetry constraints. Ref. [42] reported in 2022 that the Dirac states in antimony films are located at general momentum points.

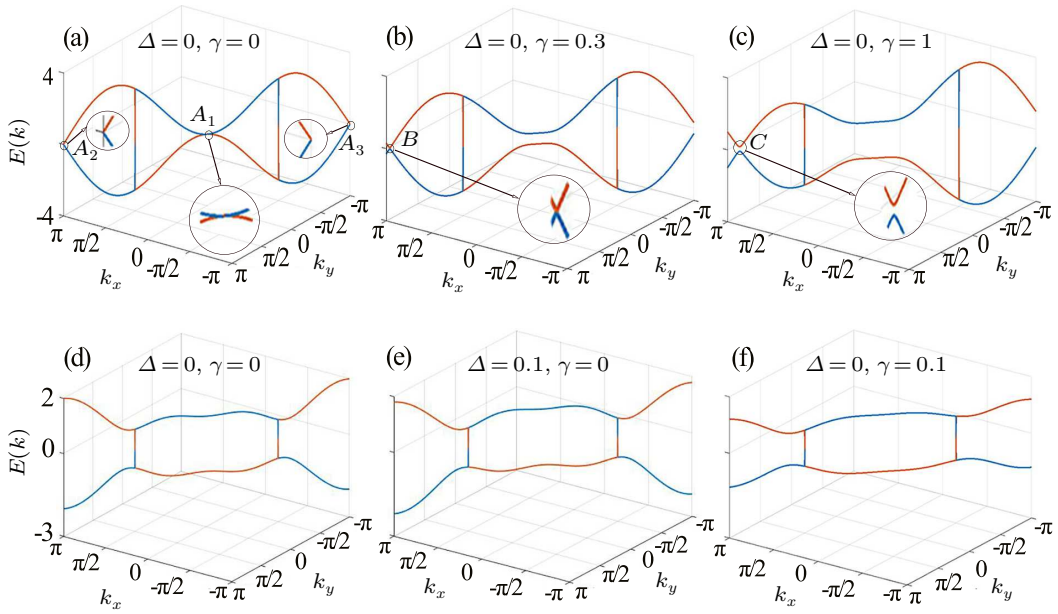


Fig. 2. The dispersion relation distribution is plotted. (a)–(c) The energy band diagrams corresponding to the imaginary coupling coefficients γ for 0, 0.3, and 1, respectively, with the remaining parameters set to $\Delta = 0$, $\delta = -1$, $t = 2$, and $\sigma = 1$. (d) and (e) The energy band curves corresponding to parameters $\delta = 0.5$, $t = 0.5$, $\sigma = 0.5$. (f) The energy band curve corresponding to parameters $\delta = 0.3$, $t = 0.5$, $\sigma = 0.3$.

A DP at a non-high-symmetry point of an optical system can be realized by adjusting the imaginary coupling coefficient in a 2D photonic crystal, as shown in Fig. 2. When the imaginary coupling coefficient increases gradually to $\gamma = 0.3$, the DP shifts from the edge of the BZ to the center of the BZ, and the DP at the center breaks. Under this condition, there is only one non-high symmetry DP, The imaginary coupling coefficient can be interpreted as a phase factor that modifies the hopping amplitude between neighboring sites in the photonic crystal. This phase factor violates the time-reversal symmetry and leads to a non-reciprocal propagation of light. Consequently, the dispersion relation is distorted and shifted by the imaginary coupling coefficient. The DP, which is a degenerate point of two bands with opposite parity, is sensitive to the phase factor and can be manipulated or split by tuning the imaginary coupling coefficient. The band gap, which is determined by the band inversion between the two bands, is also influenced by the imaginary coupling coefficient. When the imaginary coupling coefficient is sufficiently large, the band inversion can be reversed and the band gap can be opened. as shown in Fig. 2(b). When the imaginary coupling coefficient γ increases further, we find that the DP moves wholly and again breaks. The band gap widens with the rise of the imaginary coupling coefficient. By adjusting the coupling coefficient, we provide a simple model and method to locate the 2D DP at a general momentum point.

Figure 2(d) shows the band structure for $\delta = \sigma = t = 0.5$. Due to the chiral symmetry of the system, the upper and lower bands are symmetric, and there is no degenerate point in the design, only two band sharp points. When the intralayer cou-

pling coefficient $\Delta = 0.1$, the chiral symmetry of the system is broken. In Fig. 2(e), due to the breaking of chiral symmetry, the balance of the upper and lower bands is destroyed, but the two band abrupt points at $(k_x, k_y) = (\pi/2, \pi/2)$, $(k_x, k_y) = (-\pi/2, -\pi/2)$ are not broken due to the breaking of symmetry, and as Δ increases, the maximum value of the band in the range of $k_x = -\pi/2$ to $k_x = \pi/2$ and $k_y = -\pi/2$ to $k_y = \pi/2$ increases, and the maximum value of the band in the range of $k_x = |\pi/2|$ to $k_x = |\pi|$ and $k_y = |\pi/2|$ to $k_y = |\pi|$ decreases. By adjusting the coupling coefficient, we provide a simple model and method to make the 2D DP at a general momentum point.

When the system is in the topologically non-trivial state corresponding to $C = -1$, the band structure shows that, compared with the topological state corresponding to $C = -2$, the overall dispersion relation decreases inward, and the maximum value of the dispersion relation is lower. Nevertheless, the broadband sharp points do not disappear, as shown in Fig. 2(f).

A comparison of the six band diagrams reveals that there are always two sharp points in each band and that their positions do not depend on the imaginary coupling coefficient γ. The analytical solution indicates that the strong points are located at $(k_x, k_y) = (\pi/2, \pi/2)$ and $(k_x, k_y) = (-\pi/2, -\pi/2)$.

3. Research on topological states

However, not all topological systems exhibit consistent boundary state behavior under open boundary conditions.[43,44] Therefore, in specific studies, the system structure and boundary conditions must be considered to determine the energy spectrum of topological systems under open boundary conditions.

When the intralayer coupling coefficient $\Delta = 0$ and the other coupling coefficients are $\gamma = 0$, $\delta = 0.5$, $t = 0.5$ and $\sigma = 0.5$, the system is in the topological state when Chern number $C = -2$. Figure 3(a) shows the energy spectrum structure of the system with an open boundary in the y direction and an even number of lattice points, assuming $n_y = 40$ and $N_y = 80$. There are zero energy degenerate bands in the energy spectrum of the system and several particular degenerate points in the bulk state. The numerical solution indicates that the positions of these points are $k_x = \pm 1.04, \pm 2.08$, where there are four-fold degeneracies of n_y and the intracell coupling $u_\pm$ vanishes, that is, $t + 2\delta \cos k_x \pm i\gamma = 0$, as shown by the blue dashed line and the intersection point with the bulk state. If an odd number of lattice points $N_y = 81$ is chosen in the y direction, a flat band appears in the open boundary energy spectrum throughout the BZ, as shown in Fig. 3(d).

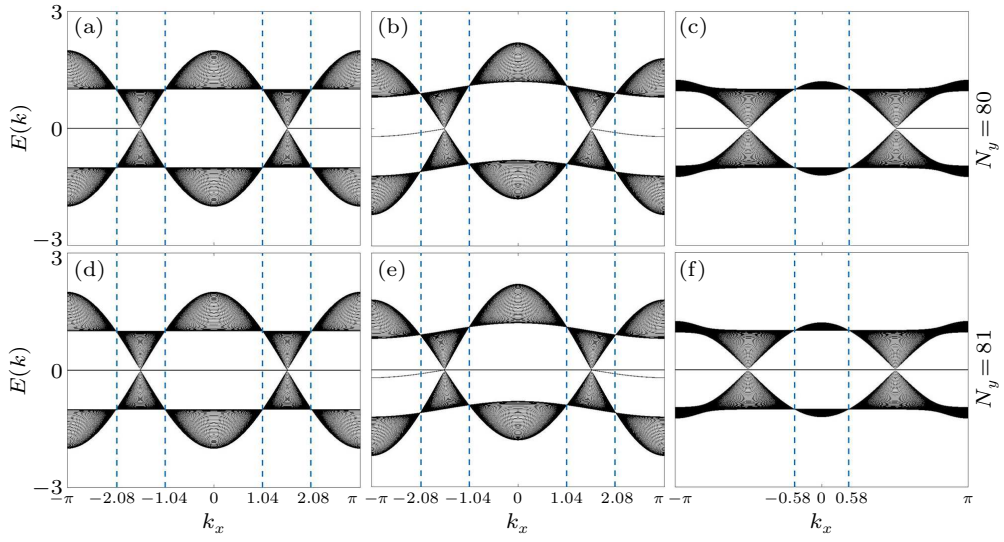


Fig. 3. Spectral distribution of topological states. (a) and (d) The open boundary energy spectrum corresponding to the topological state with Chern number $C = -2$ when $\Delta = 0$. (b) and (e) The open boundary energy spectrum of the system at $\Delta = 0.1$, compared with (a) and (d). The rest of the parameters for $\gamma = 0$, $\delta = 0.5$, $t = 0.5$, $\sigma = 0.5$. (c) and (f) The open boundary energy spectrum corresponding to the topological state with Chern number $C = -1$; parameters for $\Delta = 0$, $\delta = \sigma = 0.3$, $\gamma = 0.1$, $t = 0.5$.

When the intralayer coupling coefficient $\Delta = 0.1$, figures 3(b) and 3(e) show the change of the energy spectrum structure of the open boundary in the y direction when the intralayer coupling coefficient $\Delta \neq 0$. Figure 3(b) is the energy band diagram when the number of lattice points is even ($N_y = 80$), indicating that when the intralayer coupling coefficient Δ changes within a small range, it has a particular impact on the energy spectrum of the whole system. First, it changes the edge state of the system, making it from a topologically protected zero mode to a topologically protected near-zero way; second, it changes the symmetry of the system, making the upper and lower energy spectra no longer symmetrical but does not affect the position of the degenerate points in the bulk state. The bulk state is still decayed at $k_x = \pm 1.04, \pm 2.08$. For the energy band diagram with an odd number of lattice points ($N_y = 81$), the change of the energy spectrum diagram

is consistent with Fig. 3(d), and a zero-energy flat band appears throughout the BZ. The appearance of these states is closely related to the specific shape and topological properties of the lattice. However, increasing the number of lattice points does not change the existence and position of bulk degenerate points and topological edge states because the appearance of these states depends on the specific shape and topological characteristics of the lattice rather than just the increase in the number of lattice points.

In general, the intralayer coupling coefficient Δ affects the edge state of the system: when the intralayer coupling coefficient $\Delta = 0$, the edge state of the system is a topologically protected zero mode; when the intralayer coupling coefficient $\Delta \neq 0$, the edge state of the system is a topologically protected near-zero mode.

The number of lattice points in the y direction affects the appearance of the zero-energy flat band in the open boundary energy spectrum, regardless of whether the system is topologically trivial or non-trivial. No flat band appears in the whole space when the number of lattice points in the y direction is even. When the number of lattice points in the y direction is odd, the zero-energy flat band always exists, regardless of how the coupling coefficients change.[45,46] In summary, we propose a method to realize a flat band at a single lattice point without considering the amplitude and phase of the lattice points.

Figure 3 has simplified the 2D photonic crystal into a 1D non-reciprocal narrow-band chain model along the y direction. This narrow-band chain model simulates the light wave transmission behavior.

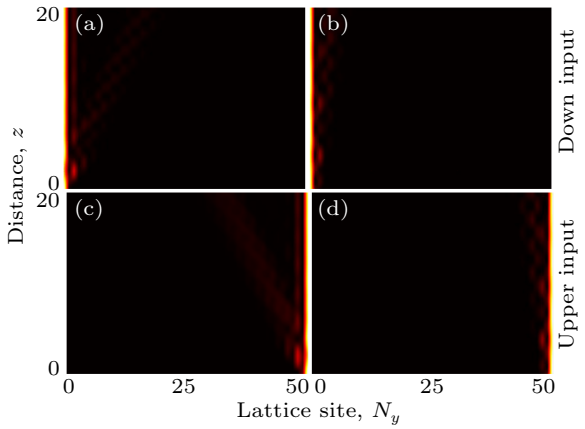


Fig. 4. Numerical simulation of topological states. (a) and (c) The light wave dynamics process of the topological edge state of the system when the Chern number $C = -2$, parameters for $\Delta = 0$, $\delta = 0.5$, $t = 0.5$, $\sigma = 0.5$, $\gamma = 0$. (b) and (d) The light wave dynamics process of the topological edge state of the system when the Chern number $C = -1$, parameters for $\Delta = 0$, $\delta = 0.3$, $t = 0.5$, $\sigma = 0.3$, $\gamma = 0.1$.

Figure 4 illustrates the light wave transmission process at the boundary of a finite system under the topologically non-trivial condition. Assuming $y = 25$, the number of lattices is $N_y = 2n_y = 50$, the wave vector $k_0 = \pi$, and a Gaussian wave packet is used for excitation. Figures 4(a) and 4(c) show the evolution of the edge states under topological non-trivial condition when the system's Chern number $C = -2$, with the coupling coefficients $\Delta = 0$, $\delta = 0.5$, $t = 0.5$, $\sigma = 0.5$, $\gamma = 0$. We observe topological edge states at the upper and lower waveguide edges, and the waveguide is localized on the outermost waveguide. Figures 4(b) and 4(d) show the evolution of the edge states under topological non-trivial condition when the system's Chern number $C = -1$, with the coupling coefficients $\Delta = 0$, $\delta = 0.3$, $t = 0.5$, $\sigma = 0.3$, $\gamma = 0.1$. We observe that the light wave oscillates and couples with other waveguides, but due to the topological property of the system, the light wave eventually localizes on the edge waveguide, which is the topological edge state.

4. Study on group velocity control

This section investigates how to control the photonic crystal's group velocity by tuning the system's coupling coefficients. The group velocities k_x and k_y of the wave packet along the x and y directions, respectively, are obtained by solving the first-order derivatives of Eq. (8) concerning v_{k_x} and v_{k_y}.

The formula for the group velocity v_{k_x} is derived as follows:

$$v_{k_x} = \frac{\mathrm{d}E_{\pm}}{\mathrm{d}k_x} = \frac{\sin k_x A}{\sqrt{\mathrm{e}^{\mathrm{i}k_y}(B+C+D+E)}}, \tag{9}$$

where $A = (-2\Delta \pm (1+\mathrm{e}^{\mathrm{i}k_y})^2 t(\delta-\sigma) - (-1+\mathrm{e}^{2\mathrm{i}k_y})\mathrm{i}\gamma\sigma \mp 4(\mathrm{e}^{\mathrm{i}k_y}\delta - \sigma)(-\delta + \mathrm{e}^{\mathrm{i}k_y}\sigma)\cos k_x))$, $B = \mathrm{e}^{2\mathrm{i}k_y}(t + \mathrm{i}\gamma + 2\delta\cos k_x)(t - 2\sigma\cos k_x)$, $C = \mathrm{e}^{\mathrm{i}k_y}(2t^2 + \gamma^2 + 2(\delta^2+\sigma^2))$, $D = 4t(\delta-\sigma) + 4t(\delta-\sigma)\cos k_x + 2(\delta^2+\sigma^2)\cos 2k_x)$, $E = t^2 - \mathrm{i}\gamma t - 2\delta\sigma + 2t\delta\cos k_x + 2\mathrm{i}\gamma\sigma\cos k_x$.

Figure 5 shows how tuning γ, an imaginary coupling coefficient in our system, affects group velocities along x. Figures 5(a)–5(c) illustrate how v_{k_x} varies with k_x for different values of γ. When $\gamma = 0$, there are three points where $v_{k_x} = 0$, corresponding to the edge and center of the BZ. The band jump point in the band structure remains a discontinuity in v_{k_x} regardless of γ. When $\gamma = 0.3$, v_{k_x} changes slightly: it becomes flatter around the center point and reaches higher maxima and lower minima. As γ increases further, these trends continue: v_{k_x} becomes more gentle at the center and more extreme at other points. Increasing γ does not affect the zero group velocity points. Still, it causes v_{k_x} to increase or decrease continuously depending on k_x and become flatter at the center. Figure 5(d) shows v_{k_x} under topological conditions. There are still three points where $v_{k_x} = 0$, as in the non-topological case, but there is no abrupt change at the band jump point; instead, two group velocity bands intersect at $(k_x, k_y, v_{k_x}) = (\pm\pi/2, \pm\pi/2, 0)$. The overall variation of v_{k_x} is also significantly reduced due to topological suppression.

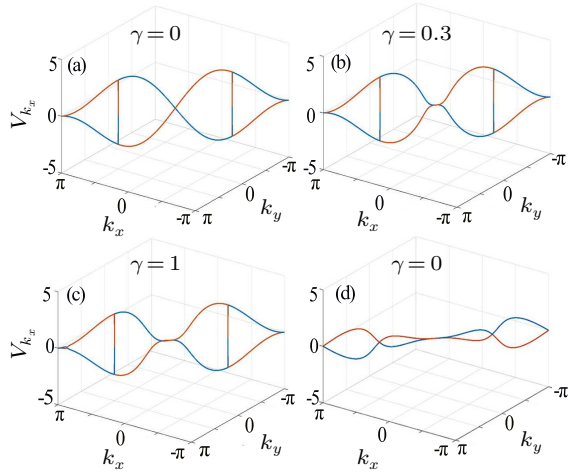


Fig. 5. Group velocity control in the x direction. (a)–(c) The group velocity variation curves for the topologically trivial state, with the same parameters as Figs. 2(a)–2(c). (d) The group velocity variation curve for the topologically non-trivial state, with the same parameters as Fig. 2(d).

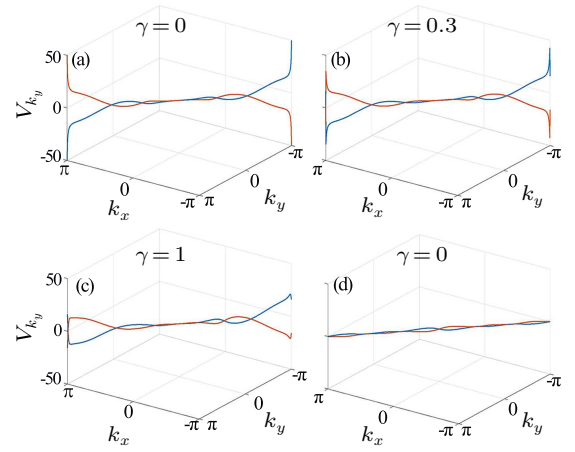


Fig. 6. Group velocity control study in the y direction. (a)–(c) The group velocity variation curves for the topologically trivial state, with the same parameters as Figs. 2(a)–2(c). (d) The group velocity variation curve for the topologically non-trivial state, with the same parameters as Fig. 2(a).

The formula for the group velocity v_{k_y} is derived as follows:

$$v_{k_y} = \frac{\mathrm{d}E_{\pm}}{\mathrm{d}k_y} = \frac{\mathrm{e}^{\mathrm{i}ky}\mathrm{i}su_+ - \mathrm{e}^{-\mathrm{i}ky}\mathrm{i}su_-}{2\sqrt{s^2 + \mathrm{e}^{\mathrm{i}ky}su_+ + \mathrm{e}^{-\mathrm{i}ky}su_- + u_+u_-}}. \quad (10)$$

Figure 6 shows the group velocity variation curve in the y direction. Figures 6(a)–6(c) illustrate how increasing γ affects v_{k_y}. Unlike v_{k_x}, v_{k_y} is not zero at the edge of the BZ; it has a value of 50 when $\gamma = 0$. As γ increases, v_{k_y} decreases at most points except for the center point, where it remains zero. The slope around this point is also tiny and close to zero, which may result in localized or dispersion-less transmission of light waves. In addition, v_{k_y} is negative for most values of k_y in in the range of 0 to π, indicating group velocity deceleration. Thus, we observe group velocity acceleration, deceleration, and zero group velocity within one period. Increasing γ does not change these phenomena significantly; it only causes v_{k_y} to decrease further. Figure 6(d) shows v_{k_y} under topological conditions. The variation of v_{k_y} is tiny under this condition; only near $(0,0)$ is there a noticeable curvature that may cause light wave diffraction due to topological suppression of group velocity variation.

5. Conclusion

As one of the most attractive optical systems for light manipulation, non-reciprocal photonic lattices provide abundant means to realize the topological edge states and regulate the group velocity. This paper presents a theoretical design of the non-reciprocal Hermite 2D photonic lattice, and the topological phase transition, topological edge state, optical transport behavior, and group velocity change in the non-reciprocal coupling photonic lattice are studied. The research results show that when the imaginary coupling coefficient $\gamma < 0.3$ and interlayer coupling coefficient $\delta < 0.5$, the system has a topologically non-trivial state of $C = -1$; when the imaginary coupling coefficient $\gamma = 0$ and the interlayer $\delta = 0.5$, the system has a topologically non-trivial state of $C = -2$. When the imaginary coupling coefficient $\gamma = 0$, the system energy band is symmetric relative to the wave vector $(k_x, k_y) = (0,0)$. In a finitely large system, the system has a zero-energy flat-top band when the lattice number in the direction y is odd. The study of group velocity shows that zero group velocity points exist regardless of the topological property of the system. However, the topological state can suppress the amplitude of the group velocity profile. To sum up, this work realizes different topological states of system and localized states of light waves in 2D photonic lattices, enriches the connotation of optical transmission and group velocity regulation in 2D non-reciprocal Hermitic photonic lattices, and has particular theoretical guiding significance in the fields of optical communication and photonic device fabrication.[47,48]

Acknowledgment

Project supported by the National Natural Science Foundation of China (Grant No. 12174307).

References

[1] Xiao D, Jiang J, Shin J H, Wang W B, Wang F, Zhao Y F, Liu C, Wu W, Chan M H W, Samarth N and Chang C Z 2018 *Phys. Rev. Lett.* **120** 056801
[2] Su W P, Schrieffer J R and Heeger A J 1979 *Phys. Rev. Lett.* **42** 1698
[3] Hao X, Wu W, Zhu J, Song B, Meng Q, Wu M,Hua C, Yang S A and Zhou M 2022 *J. Phys. Condens. Matter* **34** 255504
[4] Heide C, Kobayashi Y and Baykusheva D R, Jain D, Sobota J A, Hashimoto M, Kirchmann P S, Oh S, Heinz T F, Reis D A and Ghimire S 2022 *Nat. Photonics* **16** 620624
[5] Khanikaev A B and Shvets G 2017 *Nat. Photonics* **11** 763773
[6] Zhen B and Redondo A B 2022 *Nat. Commun.* **13** 2249
[7] Price H, Chong Y, Khanikaev A, Schomerus H, Maczewsky L J, Kremer M, Heinrich M, Szameit A, Zilberberg O and Yang Y 2022 *J. Phys. Photonics* **4** 032501
[8] Kawabata K, Higashikawa S, Gong Z, Ashida Y and Ueda M 2019 *Nat. Commun.* **10** 297
[9] Han S H, Jeong S G, Kim S W, Kim T H and Cheon S 2020 *Phys. Rev. B* **102** 235411

[10] Zhong J, Wang K, Park Y, Asadchy V, Wojcik C C, Dutt A and Fan S 2021 *Phys. Rev. B* **104** 125416
[11] Kim M, Jacob Z and Rho J 2020 *Light Sci. Appl.* **9** 130
[12] Dong J W, Chen X D, Zhu H, Wang Y and Zhang X 2017 *Nat. Mater.* **16** 298302
[13] Bernevig B A and Zhang S C 2006 *Phys. Rev. Lett.* **96** 106802
[14] Parappurath N, Alpeggiani F, Kuipers L and Verhagen E 2020 *Sci. Adv.* **6** 10
[15] Yin J, Tan C, Barcons-Ruiz D, *et al.* 2022 *Science* **375** 1398
[16] Cheng H, Sha Y, Liu R, Fang C and Lu L 2020 *Phys. Rev. Lett.* **124** 104301
[17] Cai X, Ye L, Qiu C, Xiao M, Yu R, Ke M and Liu Z 2020 *Light Sci. Appl.* **9** 38
[18] Kominis Y, Bountis T and Flach S 2016 *Sci. Rep.* **6** 33699
[19] Zhang W, Di F, Zheng X, Sun H and Zhang X 2017 *Nat. Commun.* **14** 1083
[20] Drozdov I K, Alexandradinata A, Jeon S, Nadj-Perge, S, Ji H, Cava R J, Bernevig A B and Yazdani A 2014 *Nat. Phys.* **10** 664669
[21] Zhou P, Liu G G, Ren X, Yang Y, Xue H, Bi L, Deng L, Chong Y and Zhang B 2020 *Light Sci. Appl.* **9** 133
[22] Xie B Y, Su G X, Wang H F, Su H, Shen X P, Zhan P, Lu M H, Wang Z L and Chen Y F 2019 *Phys. Rev. Lett.* **122** 233903
[23] Chen Y F, Lan Z H and Zhu J 2022 *Phys. Rev. Appl* **17** 054003
[24] Chen Y F, Meng F, Lan Z H, Jia B H and Huang X D 2021 *Phys. Rev. Appl* **15** 034053
[25] Chen Y F, Lan Z H and Zhu J 2022 *Nanophotonics* **11** 1345
[26] Chen Y F, Meng F, Jia B H, Li G Y and Huang X D 2019 *Phys. Status Solidi RRL* **13** 1900175
[27] Feng L, El-Ganainy R and Ge L 2017 *Nat Photonics* **11** 752
[28] Jiang J R, Chen W T and Chern R L 2020 *Sci. Rep.* **10** 15726
[29] Hao X, Wu W, Zhu J, Song B, Meng Q ,Wu M ,Hua C, Yang S A and Zhou M 2022 *J. Phys. Condens. Matter 34* 255504
[30] Heide C, Kobayashi Y, Baykusheva D R, *et al.* 2022 *Nat. Photonics* **16** 620624
[31] Wang Z, Chong Y, Joannopoulos J D and Soljačić M 2009 *Nature* **461** 772
[32] Du L, Hasan T, Castellanos-Gomez A, Liu G B, Yao Y, Lau C N and Sun Z 2021 *Nat. Rev. Phys.* **3** 193206
[33] Bao L, Qi B, Dong D and Nori F 2021 *Phys. Rev. A* **103** 042418
[34] Wang X, Li Y, Hu X, Gu R, Ao Y, Jiang P and Gong Q 2022 *Phys. Rev. A* **105** 023531
[35] Parappurath N, Alpeggiani F, Kuipers L and Verhagen E 2020 *Sci. Adv.* **6** 10
[36] Chen J, Liang W and Li Z Y 2019 *Phys. Rev. B* **99** 014103
[37] Mukherjee S and Rechtsman M C 2021 *Phys. Rev. X* **11** 041057
[38] Sounas D L and Alù A 2017 *Nat. Photonics* **11** 774
[39] Jotzu G, Messer M, Desbuquois R, Lebrat M, Uehlinger T, Greif D and Esslinge T 2014 *Nature* **515** 237
[40] Wang B K, Zhou X, Lin H and Bansil A 2021 *Phys. Rev. B* **104** L121108
[41] Lu Q, Cook J, Zhang X, Chen K Y, Snyder M, Nguyen D T, Reddy P V S, Qin B, Zhan S, Zhao L D, Kowalczyk P J, Brown S A, Chiang T C, Yang S A, Chang T R and Bian G 2022 *Nat. Commun.* **13** 4603
[42] Fan H, Xia B, Tong L, Zheng S and Yu D 2019 *Phys. Rev. Lett.* **122** 204301
[43] Su Z, Kang Y, Zhang B, Zhang Z and Jiang H 2019 *Chin. Phys. B* **28** 117301
[44] Bhattacharya A and Pal B 2019 *Phys. Rev. B* **100** 235145
[45] Zhang C X and Xu X S 2012 *Chin. Phys. B* **21** 044213
[46] Padavić K, Suraj S. Hegde, DeGottardi W and Vishveshwara S 2018 *Phys. Rev. B* **98** 024205
[47] Hu X X, Wang Z B, Zhang P, Chen G J, Zhang Y L, Li G, Zou X B, Zhang T, Tang H X, Dong C H, Guo G C and Zou C L 2021 *Nat. Commun.* **12** 2389
[48] El-Ganainy R, Eisfeld A, Levy M and Christodoulides D N 2013 *Appl. Phys. Lett.* **103** 161105
[49] Fukui T, Hatsugai Y and Suzuki H 2005 *J. Phys. Soc. Jpn.* **74** 1674